Combination of hysteresis models for accuracy improvement and stabilised electromagnetic calculations

Anastassios Skarlatos, Benjamin Ducharne

Combination of hysteresis models for accuracy improvement and stabilised electromagnetic calculations

Anastassios Skarlatos[a,*], Benjamin Ducharne[b,c]

[a] *Université Paris-Saclay, CEA, List, F-91120, Palaiseau, France*
[b] *Laboratoire de Génie Electrique et Ferroélectricité – INSA de Lyon, Villeurbanne, France*
[c] *ELyTMaX UMI 3757CNRS – Université de Lyon – Tohoku University, International Joint Unit, Tohoku University, Sendai, Japan*

Abstract

An interpolation strategy based on pre-evaluated integrals of the first-order reversal curves is presented. The proposed approach allows the seamless integration of different hysteresis models into a single calculation in a way that the most appropriate curve is picked up for particular subdomains of the Preisach plane. It can be shown that this approach can contribute to the stabilisation of numerical field calculations.

Keywords: hysteresis, first order reversal curves, Preisach plane, Jiles-Atherton model, Rayleigh model.

1. Introduction

A variety of ferromagnetic hysteresis models exists, the Preisach [1] or the Jiles–Atherton [2] models being the most popular ones among others [3, 4]. Each model has its merits but also serious drawbacks, such as the congruency property of the Preisach model or the incorrect representation (accommodation) of the minor loops with the Jiles-Atherton model. Even if solutions exist to better represent the minor loops like in [5, 6], they involve a larger number of parameters. These flaws can be more or less detrimental depending on the specific application we are looking at. The congruency property of the Preisach model for example becomes prohibitive for its use for incremental permeability calculations [5]. Another serious limitation are instabilities that are introduced in the numerical solver when a hysteresis model is coupled with the Maxwell equations in order to treat electromagnetic problems involving ferromagnetic media.

For all this reasons, it would be advantageous if one could couple different hysteresis models to characterise a specific material by switching to the most appropriate model in order to describe specific families of sub-curves (e.g. major loop, minor loops, weak field domain etc.). To proceed to such a hybridisation, the whole family of hysteresis curves must be first parametrised and described in some appropriate mathematical space. The coordinates of the first reversal point combined with the external field H can be used as coordinates for such a space since they provide a unique description of the magnetic state in accordance with Madelung's rules [7]. The corresponding model will be then constructed by pre-evaluation of hysteresis at specific sample points of the domain using the most appropriate model. The thus obtained hysteresis representation is closely related to the first-order reversal curve (FORC) diagrams, where the permeability values are integrated along the path up to the current H value [1].

The herein proposed approach has been applied in the case of a structural steel, where the Jiles–Atherton model has been combined with the Rayleigh model in the weak field domain and integrated in a numerical code for solving the induction problem in a thin plate. The specific steel grade is a material of intermediate hardness, and has been selected as study material because of its common use in many practical applications. It turns out that the combination of the two models succeeds in stabilising the numerical solution and a very good agreement with experimental measurements is achieved.

*Corresponding author: anastasios.skarlatos@cea.fr

2. Formal representation and relation to the Preisach theory

We shall restrict ourselves in this article to symmetrical loops obtained via periodic external fields. It should be noticed that the thereupon developed approach is also applicable to pulsed excitations without cross-over since only the first magnetisation curve and the descending branch are involved (i.e., no branch change is resulted). In addition, it is assumed that the magnetic field **H** and the magnetic induction **B** are parallel, which means that the material can be described by a scalar hysteresis law $B(H)$ with $B = |\mathbf{B}|$ and $H = |\mathbf{H}|$. According to the Madelung rules, each curve is completely described by the coordinates of the last reversal point [7], which, under the assumptions mentioned above, is translated to the formal relation

$$M = M(H, H_r, M_r(H_r)) \tag{1}$$

where M_r, H_r are the coordinates of the reversal point. By hypothesis, all reversal points are lying on the first magnetisation curve $M_r(H_r)$, which implies that one of the two coordinates can be dropped, so (1) reduces to the two variables expression

$$M = M(H, H_r)\,. \tag{2}$$

Drawing all possible states in the configuration plane (H, H_r), with $-H_r \leq H \leq H_r$, we end up with the triangular of Fig. 1.

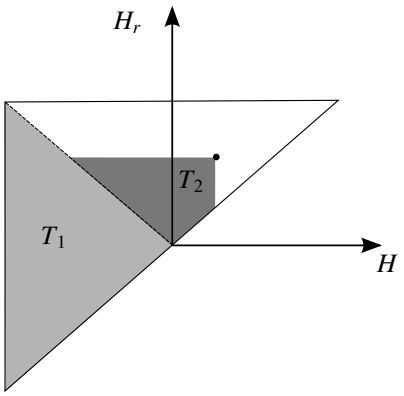

Figure 1: Cumulative FORC representation of the magnetisation M for a system with symmetrical excitation and hysteresis calculations corresponding to the different points of the configuration space.

The domain is closely related to the FORC diagram in the Preisach plane, with the difference that each point of the former corresponds to a FORC integral over the greyed domain (the sum of the light T_1 and dark grey triangle T_2 in Fig. 1) [1, 8]

$$M(H, H_r) = \int_{T_1+T_2} \rho(\alpha, \beta)\, d\alpha d\beta \tag{3}$$

with

$$\rho(\alpha, \beta) = -\frac{1}{2}\frac{\partial^2 M_{FORC}}{\partial H_r \partial H}. \tag{4}$$

It is recalled the T_1 domain stands for the demagnetisation procedure that has to be followed in order to drive the material to its demagnetised state [1]. Although equivalent to the FORC representation, it turns out that working with integrated variables gives us enhanced flexibility to focus on parts of the domain where specific features are sought and to calculate the inverse curves. These two topics will be subject of the next paragraphs.

3. Case of interest: small-field limit of the Jiles–Atherton model

Models that have been identified using the major hysteresis curves usually perform badly at the small field domain. This is particularly true for the JA model, which is notoriously unstable in the small field domain if no special action is taken in its initial description [6].

Since we will use this particular model as example, the JA expression for the differential magnetic susceptibility is given for convenience

$$\frac{dM}{dH} = \frac{1}{1+c}\frac{M_a - M}{\left(c\frac{\delta k}{\mu_0} - \alpha\right)(M_a - M)} + \frac{c}{1+c}\frac{dM_a}{dH} \tag{5}$$

where M_a is the anhysteretic curve, whose relation with H is, in most cases, approximated by Langevin's function

$$M_a = M_s\left[\coth(H_e/a) - a/H_e\right]. \tag{6}$$

μ_0 is the magnetic permeability of the free space, δ is a sign parameter that defines the working branch $\delta = \text{sign}(dH/dt)$ and M_s, a, α, k, c are the model parameters determined by identification. Other relations of this differential susceptibility can be found in the literature. They would adapt to the proposed method just as well.

A possible remedy for improving the low field behaviour is to couple the model with the Rayleigh formula, which is very robust and precise in this domain.

$$M_{Ray}(H, H_r) = (\chi_{in} + \nu H_r) + \frac{\nu}{2}\left(H_r^2 - H^2\right). \tag{7}$$

The multidimensional representation of the hysteresis considered here is particularly well suited for coupling a given hysteresis model (like the JA model in this case) with an asymptotic expression by locally replacing the corresponding part of the $B(H, H_r)$ domain. The principle is illustrated in Fig. 2. Defining a transition threshold for the reversal field value H_r (in this particular example,

it has been chosen as the 10% of the maximum field value H_m, i.e. $H_r = H_m/10$), we replace the M values lying in the domain $H_r \leq H_t$ with the ones calculated using the Rayleigh expression.

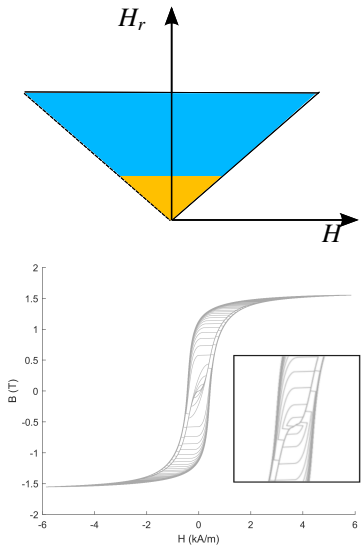

Figure 2: (Upper panel) Support of the JA model (in light blue) and Rayleigh expression (in orange) for the coupled model in the (H, H_r) plane. (Lower panel) Resulting family of inner curves. The inset shows a zoom of the low-field curves obtained if only the JA model is employed. The improvement achieved via the application of the Rayleigh expression is demonstrated by comparing with the inner loops of the main figure.

Assuming that the principle model has been identified using one or a set of external curves, we need also to determine the Rayleigh model parameters χ_{in} and ν. Their values are obtained by imposing the continuity of the magnetisation and its derivative (i.e., the differential susceptibility) at the transition threshold, namely:

$$M_{Ray}(H_t) = M_{JA}(H_t) \tag{8}$$

$$\chi_{Ray}(H_t) = \chi_{JA}(H_t) \tag{9}$$

This procedure can be imagined being extended for hyrbridising the basic hysteresis model with other asymptotic expressions, models, or even experimental curve sets in specific subdomains of the (H, H_r) plane. In that way $M(H, H_r)$ can be viewed as a generic hysteresis meta-model [9].

4. Numerical evaluation

Having defined the magnetisation function $M(H, H_r)$, we shall focus now on the details of its numerical evaluation. Introducing a computational mesh G spanning the (H, H_r) domain, the magnetisation function is evaluated at each node thus yielding a set of numerical values

$$M^{(i)} = M\left(H^{(i)}, H_r^{(i)}\right). \tag{10}$$

The magnetisation value at all intermediate points is simply obtained by interpolation, namely:

$$M(H, H_r) = \sum_{i \in G} c_i w_i(H, H_r) \tag{11}$$

where $w_i(H, H_r)$, $\forall i \in G$ is the interpolation basis and c_i the expansion coefficients, which are evaluated by imposing the fulfilment of (10) at the grid nodes. In its simplest form, it can be formed by polynomial expressions with global or local support or more sophisticated elements like radial basis functions etc. [10].

When we are interested in the solution of the field problem, where B instead of H is the variable of interest, we need an inverse relation that maps B to H. Although efficient approaches have been proposed in the literature for the JA inversion [11], a straight-forward numerical inversion can be applied with this particular approach. Noting that the right-hand side can be formally written $M\left(H^{(i)}, H_r^{(i)}\right) = M\left(H^{(i)}, H_r\left(M_r^{(i)}\right)\right) = M\left(H^{(i)}, M_r^{(i)}\right)$ and using the magnetic constitutive relation, $B = \mu_0 (H + M)$, (10) becomes

$$B^{(i)} = B\left(H^{(i)}, B_r^{(i)}\right). \tag{12}$$

The inverse relation is then obtained by permutation of the discrete sets $\left(B^{(i)}, H^{(i)}, B_r^{(i)}\right) \rightarrow \left(H^{(i)}, B^{(i)}, B_r^{(i)}\right)$, with magnetic field values at the intermediate points been given by a similar interpolation relation with (11).

5. Solution of the field problem: the evolution operator

The (B, B_r) representation approach of the hysteresis operator also facilitates the solution of the field problem when ferromagnetic materials with hysteresis are involved. When solving Maxwell's equations is usually preferable to work with the vector magnetic potential $\mathbf{A}$ instead of the magnetic induction $\mathbf{B}$ with the two quantities being related via the equation

$$\mathbf{B} = \nabla \times \mathbf{A}. \tag{13}$$

which holds as definition relation of $\mathbf{A}$. Let us consider a uniform discretisation of the time axis $t_n = n\Delta t$ with $n = 1, 2, \ldots N$ and Δ a constant time step. We define the state vector $(\mathbf{A}_n, \mathbf{A}_n^r)^T$, where $\mathbf{A}_n$ and $\mathbf{A}_n^r$ are the potential value and the potential that corresponds the reversal magnetic

induction at the nth timestep. $\mathbf{A}_n$ is obtained by integrating Maxwell's equations using an implicit Euler scheme and a fixed-point approach for the linearisation of the material operator [12, 13].

$$\nabla\times\mu_0^{-1}\nabla\times\mathbf{A}_n+\frac{\sigma}{\Delta t}\mathbf{A}_n=\frac{\sigma}{\Delta t}\mathbf{A}_{n-1}+\mathbf{J}_n+\nabla\times\hat{\mathbf{M}}\left(\mathbf{A}_n,\mathbf{A}_{n-1}^r\right). \tag{14}$$

where σ is the piece conductivity, and $\mathbf{J}_n$ is the excitation current density. $\hat{\mathbf{M}}(\mathbf{A}_n,\mathbf{A}_n^r)$ stands or the magnetisation function which is expressed in terms of the state variables. It is formally related to the magnetisation operator described above via the relation

$$\hat{\mathbf{M}}(\mathbf{A}_n,\mathbf{A}_n^r)=\mathbf{M}(\nabla\times\mathbf{A}_n,\nabla\times\mathbf{A}_n^r). \tag{15}$$

Since we have restricted ourselves in this work to scalar hysteresis law, $\mathbf{M}$ should be understood acting on the magnetic potential modulus instead of the potential itself, i.e. $\mathbf{M}=\mathbf{M}\left(|\nabla\times\mathbf{A}_n|,\left|\nabla\times\mathbf{A}_n^r\right|\right)$[1]. The generalisation to orthotropic materials where a hysteresis operator can be determined per direction is straight-forward. The general case of vector hysteresis however requires modifications to the present approach. Equation (14) is implicit in terms of the potential solution $\mathbf{A}_n$, hence it is solved iteratively. Once $\mathbf{A}_n$ is known, one can easily obtain the new value of the reversal field by examining if the $\mathbf{A}_n$ is local minimum with respect to time:

$$\mathbf{A}_n^r=\begin{cases}\mathbf{A}_{n-1}, & \text{if } \mathbf{A}_n^0=0\\ \mathbf{A}_{n-1}, & \text{if } |\nabla\times\mathbf{A}_n|<\left|\nabla\times\mathbf{A}_n^r\right|\\ \mathbf{A}_{n-1}^0, & \text{elsewhere.}\end{cases} \tag{16}$$

The update equations (14) and (16) constitute an update operator which translates the state vector at the $n-1$ timestep to the n timestep: $\mathcal{F}:\mathcal{F}\circ\left(\mathbf{A}_{n-1},\mathbf{A}_{n-1}^r\right)^T\rightarrow(\mathbf{A}_n,\mathbf{A}_n^r)^T$. A visualisation of the state vector evolution in the augmented $(\mathbf{A}_n,\mathbf{A}_n^r)^T$ space is given in Fig. 3 The state vector initially moves along the $\mathbf{A}_n=\mathbf{A}_n^r$ line (zero reversal field) up to the first reversal, where it shifts to a constant $\mathbf{A}_n^r$ line (there is one trajectory per field point). Upon the next excitation reversal (end of the half-period) the state vector shifts to the opposite, $-\mathbf{A}_n^r$, line and so on for every half-period. For illustration purposes, the trajectories are drawn for one of the potential components.

The above described approach has been tested for the calculation of the magnetic field in a thin planar ferromagnetic specimen. The examined configuration is shown in Fig. 4. The plate thickness is 1.54 mm. The plate material is a standard structural steel of intermediate hardness. Its hysteresis curves are shown in Fig. 2b. The magnetic field is excited using a pair of coaxial coils fed with a sinusoidal current. The two coils are connected in series and at opposite polarity in order to enhance the parallel to the surface magnetic field component, thus forming a kind of open half-magnetic-circuit. The coils inner and outer diameter equal to 18 and 50 mm, respectively; their length is 67 mm, and they are wound with 545 turns each. The signal frequency is 10 Hz. The magnetic field is then measured at a point lying beside the coils by means of a Hall magnetic field sensor. The comparison between simulation and measurements for different levels of excitation is shown in Fig. 5. For the purpose of comparison, the simulation results have been rescaled by a factor of 1.1, and a 4 ms shift has been introduced. It is important to note the good agreement at small amplitudes, demonstrating the hysteresis stabilisation beneficial effect with the Raleigh formula.

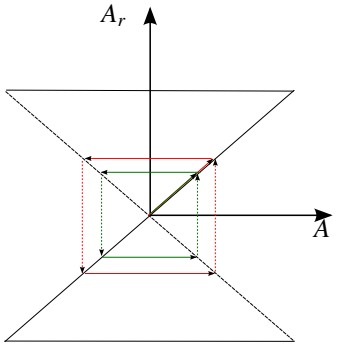

Figure 3: Trajectory of the state vector $(\mathbf{A}_n,\mathbf{A}_n^r)^T$ for a symmetric excitation. Different colours correspond to different points in the piece. The drawn trajectories must be imagined applying for each component of $\mathbf{A}$.

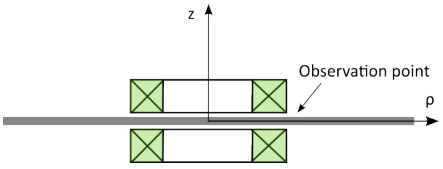

Figure 4: Measurement setup. A large (infinite) plate is excited by a pair or coaxial coils. The arrangement is described by a cylindrical coordinate system whose origin coincides with the centre of the plate.

6. Conclusions

A hysteresis representation in an augmented space spanned by the external H and the reversal H_r field has been presented. Including the reversal field as an additional axis transforms the multi-branch hysteresis function to a single

[1] At that stage, no space adaptation of the J-A model parameters have been done even if the stability of the code would allow it.

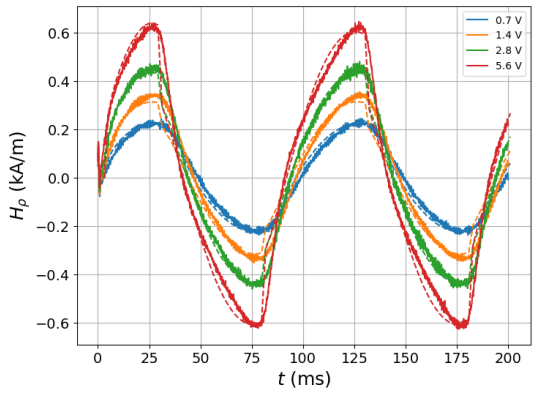

Figure 5: Comparison between simulation results and measurements for the time evolution of the tangential magnetic field component H_ρ at the observation point. Solid line: measurements, dashed line: simulation. The different colours correspond to the different values of excitation voltage. Notice the increasing distortion with growing excitation.

branch, which offers a certain convenience in the description and a seamless integration with a field solver. Combining different hysteresis models (or even experimental sets of curves) is straightforward. This latter point proves very important for the stabilisation of field calculations involving ferromagnetic materials.

In this work, only the case of symmetrical curves has been considered. Although this assumption is applicable to a large number of problems with practical interest, namely systems undergoing periodic or pulsed electromagnetic excitation it remains a special case. Systems with arbitrary excitation will necessitate a generalisation of the present approach, which will be the subject of a future work. The extension also to full vector hysteresis models is a subject worthy of investigation.

References

[1] I. Mayergoyz, Mathematical Models of Hysteresis and Their Applications, 1st Edition, Elsevier Science Inc., New York, 2003.

[2] D. C. Jiles, D. L. Atherton, Theory of ferromagnetic hysteresis 61 (1986) 48–60. doi:10.1016/0304-8853(86)90066-1.

[3] G. Mörée, M. Leijon, Review of hysteresis models for magnetic materials, Energies 16 (9) (2023) 3908.

[4] A. Iványi, Hysteresis models in electromagnetic computation, Budapest: Akadémiai Kiadó, 1997.

[5] B. Gupta, B. Ducharne, G. Sebald, T. Uchimoto, Physical interpretation of the microstructure for aged 12 Cr-Mo-V-W steel creep test samples based on simulation of magnetic incremental permeability 489 (2019) 165250. doi:10.1016/j.jmmm.2019.165250.

[6] A. Benabou, J. V. Leite, S. Clénet, C. Simão, N. Sadowski, Minor loops modelling with a modified jiles-atherton model and comparison with the preisach model 230 (2008) e1034–e1038. doi:10.1016/j.jmmm.2008.04.092.

[7] L. Dupré, J. Melkebeek, Electromagnetic hysteresis modelling: from material science to finite element analysis of devices, International Compumag Society Newsletter. 10(3). 10 (3) (2003) 4–15.

[8] A. Stancu, P. Andrei, Characterization of static hysteresis models using first-order reversal curves diagram method 372 (1) (2006) 72–75. doi:doi.org/10.1016/j.physb.2005.10.022.

[9] A. Skarlatos, A. Martínez-de Guerenu, R. Miorelli, A. Lasaosa, C. Reboud, A regressor-based hysteresis formulation for the magnetic characterisation of low carbon steels 581 (2020) 411935. doi:10.1016/j.physb.2019.411935.

[10] A. Forrester, A. Sobester, A. Keane, Engineering design via surrogate modelling: a practical guide, John Wiley & Sons, 2008.

[11] N. Sadowski, N. J. Batistela, J. P. A. Bastos, M. Lajoie-Mazenc, An inverse Jiles-Atherton model to take into account hysteresis in time-stepping finite-element calculations 38 (2) (2002) 797–800. doi:10.1109/20.996206.

[12] A. Skarlatos, T. Theodoulidis, N. Poulakis, A fast and robust semi-analytical approach for the calculation of coil transient eddy-current response above planar specimens 58 (9) (2022) 1–9. doi:10.1109/TMAG.2022.3183019.

[13] A. Skarlatos, T. Theodoulidis, Study of the non-linear eddy-current response in a ferromagnetic plate: Theoretical analysis for the 2D case 93 (Supplement C) (2018) 150–156. doi:10.1016/j.ndteint.2017.09.003.